Structural Analysis of the Anti-Malaria Active Agent Chloroquine under Physiological Conditions

Torsten Frosch,[†] Michael Schmitt,[†] Gerhard Bringmann,[‡] Wolfgang Kiefer,[§] and Jürgen Popp*[,†,⊥]

Institut für Physikalische Chemie, Friedrich-Schiller-Universität Jena, Helmholtzweg 4, D-07743 Jena, Germany, Institut für Organische Chemie, Universität Würzburg, Am Hubland, D-97074 Würzburg, Germany, Institut für Physikalische Chemie, Universität Würzburg, Am Hubland, D-97074 Würzburg, Germany, and Institut für Physikalische Hochtechnologie e.V., Albert-Einstein-Strasse 9, D-07745 Jena, Germany

Received: August 9, 2006; In Final Form: October 25, 2006

UV resonance Raman spectroscopy was applied for a selective enhancement of molecular vibrations of the important antimalarial chloroquine under physiological conditions. The resonance Raman spectra of chloroquine at pH values resembling the pH value of blood and the pH value of the acid food vacuole of plasmodium can unambiguously be distinguished via Raman resonantly enhanced mode at 721 cm^{-1}. These vibrations are assigned to -$(CH_2)_n$- rocking mode of the chloroquine side chain and are expected to be influenced by protonation of chloroquine. Furthermore, vibrations belonging to the quinoline ring (important for $\pi-\pi$-interactions to hemozoin) are resonantly enhanced and can be studied selectively. A convincing mode assignment was performed by means of DFT calculations. These calculations proved that the different protonation states of chloroquine remarkably influence various vibrational modes, the molecular geometry, and molecular orbitals. The presented results are of significant relevance for a Raman spectroscopical localization of chloroquine inside the acid food vacuole of plasmodium, the study of $\pi-\pi$-interactions of chloroquine to the biological target molecules hematin and hemozoin and the protonation state of chloroquine during this docking process. The protonation of the weak base chloroquine is considered to be crucial for an accumulation inside the acid food vacuole of plasmodium and an object for resistances against this drug.

Introduction

Malaria has existed for approximately thirty million years and antimalarials have been known for hundreds of years. Chloroquine (Figure 1), related to quinine, was discovered by Hans Andersag from Bayer Company in 1934 and was the first synthetic antimalarial produced on an industrial scale. Chloroquine became the leading antimalarial attributed to its outstanding properties and caused one the most important health advances ever achieved by a drug against an infectious disease.[1,2] Despite this public health impact and arising resistances against chloroquine on a global scale, is its mode of action on a molecular level is still not fully understood.

Chloroquine is believed to act by interfering the detoxification process of the hemoglobin digestion byproducts in the red blood cell state of plasmodium asexual life cycle.[3−9] It has been suggested that both, the quinoline ring system (via $\pi-\pi$-interaction to the porphyrin aromatic system in hemozoin) and the aliphatic side chain are crucial for the mode of action of chloroquine.[10−13] It was demonstrated that the weak basicity of the quinoline nitrogen and the tertiary amine nitrogen within the side chain are of importance for the chloroquine accumulation within the acid food vacuole of plasmodium (vacuolar accumulation ratio) via pH trapping. Furthermore, it is expected that slight alterations of the pH value within the food vacuole of plasmodium are crucial for building up resistances against chloroquine.[14−16]

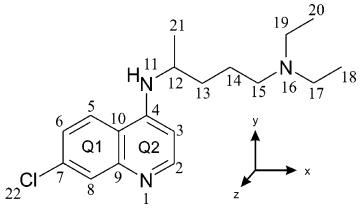

Figure 1. Molecular structure of chloroquine. The atomic numbering scheme, the partition of the quinoline ring in Q1 and Q2, and the coordinate system is used in the description of the mode assignment.

In vitro spectroscopical studies of the interactions between chloroquine and different forms of hematin (Fe(III)-protoporphyrin-IX), e.g., monomer or μ-oxo dimer, suggested that $\pi-\pi$-interactions between the quinoline ring system of the drug and the porphyrin system of the target structures are very likely to exist.[17−21] NMR investigations in combination with semiempirical calculations of complexes between chloroquine at different protonation states and the μ-oxo dimer structure of hematin revealed that the state of protonation of chloroquine plays an important role for its binding capabilities and also that the aliphatic side chain might be important for a stabilization of the drug-hematin complex.[17] Recent studies showed that chloroquine acts as a kind of tailor-made crystal growth inhibitor by selectively binding to the small active growing faces of the hemozoin crystallites, known as malaria pigment.[22,23]

In this paper a detailed resonance Raman spectroscopical study of chloroquine under physiological conditions is presented.

* Corresponding author phone: 36 41 94 8320; fax: 36 41 94 8302; e-mail: juergen.popp@uni-jena.de.
[†] Friedrich-Schiller-Universität Jena.
[‡] Universität Würzburg.
[§] Universität Würzburg.
[⊥] Institut für Physikalische Hochtechnologie e.V..

10.1021/jp065136j CCC: $37.00
Published on Web 01/26/2007

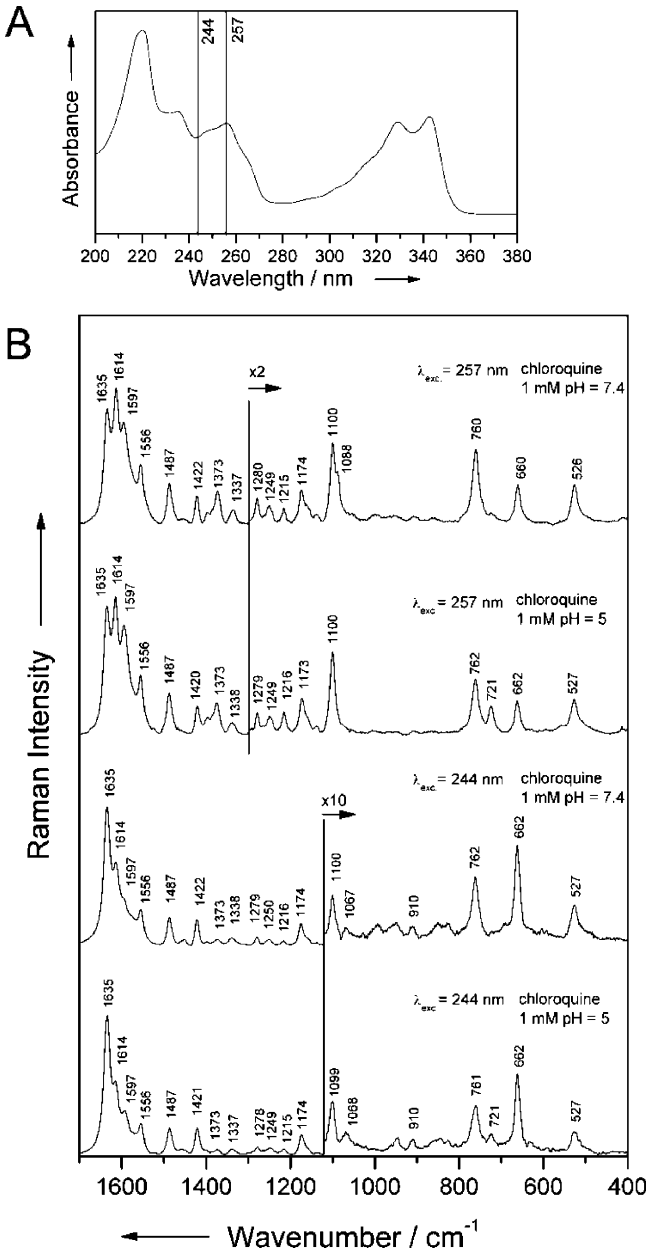

Figure 2. A: Absorption spectrum of chloroquine (1 mM solution, pH 7.4). The UV excitation wavelengths are marked as vertical lines. B: UV resonance Raman spectroscopic characterization of 1 mM solutions of chloroquine (CQ) at pH 4.7 and pH 7.4 with excitation wavelengths 244 and 257 nm. Intensities of spectra under excitation with 257 nm are stretched by factor 2 from 400 to 1300 cm^{-1} and intensities of spectra under excitation with 244 nm are stretched by factor 10 from 400 to 1120 cm^{-1} for better illustration.

It will be studied whether the characteristic molecular vibrations of chloroquine, involving molecular groups important for forming the $\pi-\pi$-interactions to hemozoin, can be selectively monitored via an enhancement by means of resonance Raman spectroscopy. The influence of two different characteristic pH values of 7.5 (pH value in blood) and 5 (pH value inside the acid food vacuole of plasmodium) onto the resonance Raman spectra of chloroquine will be investigated. A detailed assignment of the vibrational modes of chloroquine is performed by means of DFT calculations. Thus, the influences of the different protonation states of chloroquine onto its molecular geometry, molecular orbitals, and vibrational modes are studied to interpret the experimental findings.

TABLE 1: Comparison of the Relative Enhancements of Raman Bands in the Spectral Region from 1500 to 1650 cm^{-1} of Chloroquine upon Excitation with 244 and 257 nm[a]

wavenumber of Raman peak/cm^{-1}	1635	1613	1597	1575	1556
A_{244}/A_{257} at pH 7.4	4.55	1.59	1	2.13	1,67
A_{244}/A_{257} at pH 5	4.55	1.69	1	1.56	2.04

[a] The corresponding resonance Raman spectra are depicted in Figure 2B and the atomic displacements are shown in Figure 4A. The different enhancements of the peaks are expressed as A_{244}/A_{257} ratios, while A is the fitted area of the peak. The values are normalized by setting A_{244} (1597 cm^{-1})/A_{257} (1597 cm^{-1}) to 1.

Materials and Methods

Chemicals. Chloroquine diphosphate was purchased from Sigma-Aldrich and was used without further purification. Solutions of 1 mM chloroquine at distinct pH values were adjusted via a phosphate buffer. For all Raman measurements possible background signals due to the buffer were tested.

Spectroscopy. The non-resonant Raman spectrum of the pure active agent chloroquine was recorded with a Bruker FT Raman spectrometer (RFS 100/S) at the macroscopic mode with a spectral resolution of 2 cm^{-1}. A Nd:YAG laser operating at its fundamental wavelength of 1064 nm with an estimated laser power at the samples of 100 mW was used as the Raman excitation source. A liquid nitrogen cooled Ge-detector was used to collect the Raman scattered light.

The complementary FT−IR spectrum of chloroquine was measured as a KBr pellet using a Bruker IFS 66 spectrometer equipped with a DTGS (doped triglycerinsulfate) detector and with 4 cm^{-1} spectral resolution.

Resonance Raman spectroscopy was performed with a UV Raman setup (HR800, Horiba/Jobin-Yvon), equipped with a liquid N_2 cooled CCD detector. Validation of the wavenumber axis was performed via the well-known Raman signals from Teflon. The excitation wavelengths, 244 and 257 nm, are derived from an intracavity frequency doubled argon-ion laser (Innova300-MotoFreD, Coherent Inc.). The laser power at the samples was estimated to be 3 mW. The spectral resolution was 5 cm^{-1}. The 1 mM solutions of chloroquine were placed in a spinning vessel and the laser exposure time was only 150 s per measurement; to avoid any photochemical or heating effects.

Density Functional Theory Calculation. DFT calculations were performed with Gaussian 03[24] applying the hybrid exchange correlation functionals B3LYP[25−27] and B3PW91[25,28] since these functionals are well-known to provide reliable estimates of experimental wavenumbers of organic molecules, in terms of lowest root-mean-square deviations,[29−35] and to yield very accurate results with the applied split valence basis set 6-31+G(d,p).[36−38] The calculation of chloroquine in a water environment was performed within the framework of the isodensity polarized continuum model.[39] For all presented results, a finer integration grid was applied, which is essential for DFT calculations.

The DFT calculated harmonic vibrational wavenumbers are typically too large to be compared with the experimentally observed ones mainly due to neglect of anharmonicity, incomplete incorporation of electron correlation, and the use of finite basis sets. However, this problem can be circumvented by applying scaling factors to the harmonic force constant matrix. Pulay and other groups developed very successfully the application of sets of transferable scaling factors to different types of harmonic force constants in natural internal coordinates.[31−33,41−45] Such a significant improvement of the normal modes will also improve the calculated intensities; but one should keep in mind the possible source of ambiguity introduced by this approach.

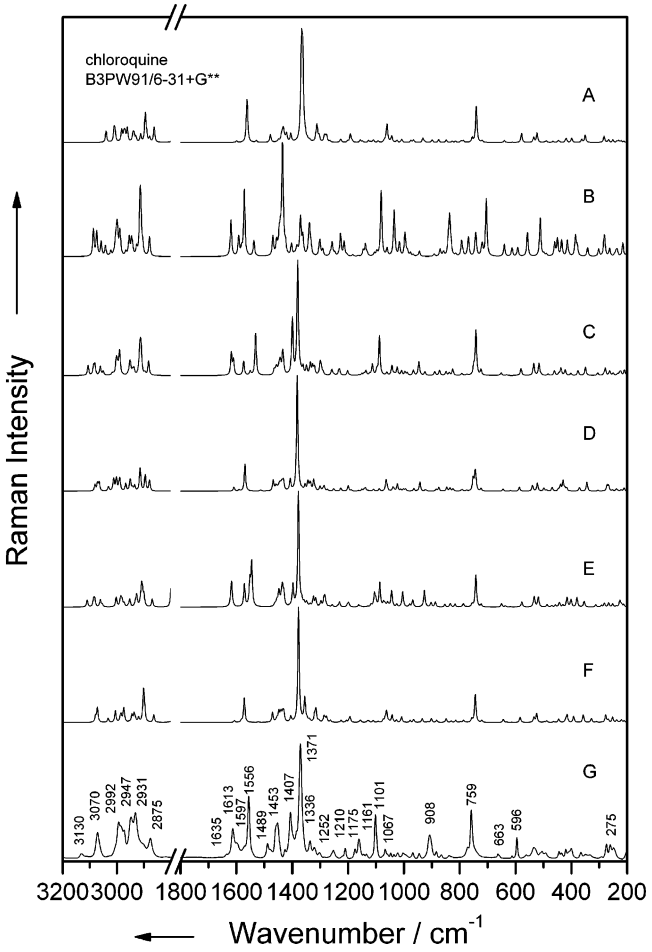

Figure 3. Comparison of the experimental Raman spectrum of chloroquine diphosphate with the calculated (B3PW91/6-31+G(d,p); scaling factors 0.965 and 0.95) Raman spectra of chloroquine (CQ) at different protonation states and in a simulated water environment. A: DFT calculation of the Raman spectrum of CQ (simulated water environment PCM-model). B: DFT calculation of the Raman spectrum of CQ protonated at N1, N16, and N11. C: DFT calculation of the Raman spectrum of CQ protonated at N1 and N16. D: DFT calculation of the Raman spectrum of CQ protonated at N16. E: DFT calculation of the Raman spectrum of CQ protonated at N1. F: DFT calculation of the Raman spectrum of CQ unprotonated. G: Experimental FT Raman spectrum of chloroquine diphosphate ($\lambda_{exc.} = 1064$ nm).

Fortunately the overestimation of the calculated harmonic vibrational wavenumbers is relatively uniform; therefore, almost the same accuracy as for scaling the harmonic force constants can be achieved by the application of transferable scaling factors directly to the harmonic wavenumbers (especially in case of B3PW91 and B3LYP).[30,39,46] It has been demonstrated that the application of two scaling factors, one for vibrations below 1800 cm^{-1} and one above 1800 cm^{-1}, lead to very good results[47,48] and this procedure was, therefore, applied in this paper. It was possible to confirm the scaling factor given by Bauschlicher et al.[47] (for B3LYP/6-31+G(d,p) 0.9781 below 1800 cm^{-1} and approximately 0.95 above 1800 cm^{-1}). For the applied hybrid functional B3PW91, values of 0.965 for modes below 1800 cm^{-1} and 0.95 above 1800 cm^{-1} were derived.

The Raman intensities were calculated from the Raman scattering activities.[49] The IR and Raman spectra with finite bandwidth were simulated by convoluting the theoretical stick spectra with a Gauss−Lorentz weighted profile.

Potential energy distribution (PED) calculations based on the Wilson GF matrix method[50] were performed with gar2ped[51] to derive a quantitative decomposition of the normal modes in intuitive internal coordinates.

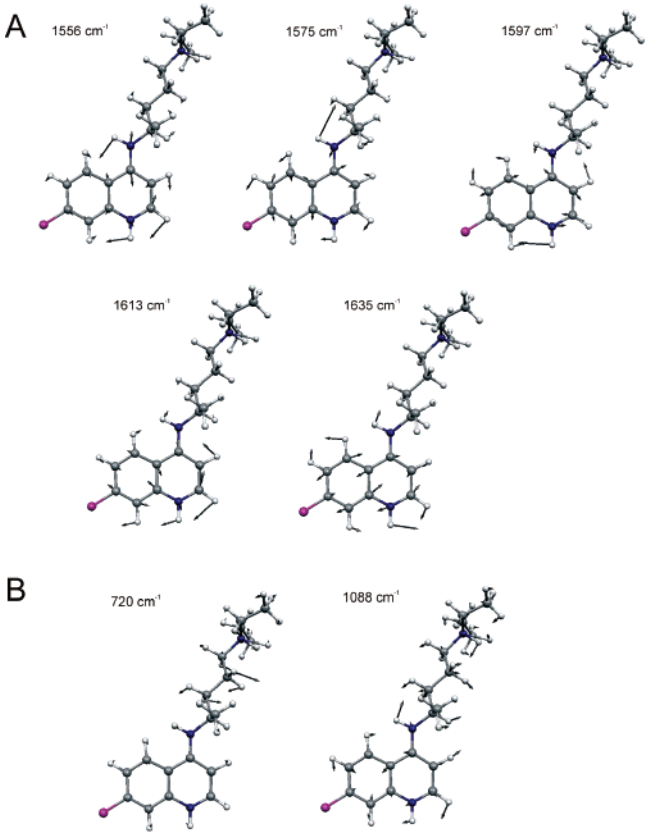

Figure 4. Atomic displacements of calculated vibrational modes of chloroquine protonated at N1 and N16 (see Figure 1). The Raman intensities of these modes are significantly different under resonance enhancement of 1 mM solutions of chloroquine at pH 5 and pH 7.4. A: These modes are assigned mostly to C=C stretching modes and C−H in plane bending modes of the quinoline ring of chloroquine. For details see text. B: These mode is assigned mostly to -(CH_2)n- rocking mode of the side chain.

Results and Discussion

UV Resonance Raman Spectroscopy. Raman spectroscopy is an extremely capable method to monitor the docking process of chloroquine to the possible hematin targets, in terms on studying the influence of the attachment on distinct molecular vibrations.[21] However, since the active agents are usually present at low concentrations (1 mM in case of chloroquine) in the acid food vacuole of plasmodium and off-resonant Raman spectroscopy suffers from low scattering cross sections, the signals must be enhanced. This can be done by utilizing the resonance Raman effect if the wavelength of the Raman excitation laser lies within an electronic absorption of the sample.[52] For the resonance Raman investigations of chloroquine presented within this study, the two deep UV excitation wavelengths at 244 and 257 nm were chosen. A major advantage of deep UV Raman spectroscopy is that Raman disturbing fluorescence interference exists very unlikely when excitation is provided at wavelengths below 250 nm because a typical Raman spectral range of 4000 cm^{-1} occurs in less than 30 nm above the excitation wavelength and fluorescence at wavelengths below 280 nm is rare. This fact, therefore, provides spectral separation of Raman and fluorescence emission bands resulting in high signal-to-noise measurements. The technique is even more appropriate since the Raman

TABLE 2: Wavenumbers and Vibrational Assignment of the Raman Spectrum of Chloroquine[a]

$\tilde{\nu}$/cm^{-1}	vibrational assignment
3130-2875	C−H stretch in quinoline (very strong at C(2), C(3), C(5), C(6)) and in side chain—prominent in-phase νCH localized at C(18)H$_3$, C(20)H$_3$, C(21)H$_3$, and at C(13)H$_2$, C(14)H$_2$
1635	a high symmetric stretching mode in quinoline ring, where νC(6)═C(5) [12%], νC(8)═C(9) [13%], νC(10)═C(4) [6%] and νN(1)═C(2) [11%] compress in phase along the nuclear bonding axis, while νC(3)═C(2), νC(10)═C(9) and νC(5)═C(10) [5%] stretch at the same time. Very strong in plane bendings takes place at C(5)C(10)C(9) [8%] and C(2)N(1)C(9) [8%] and in plane CH bendings are present around the quinoline ring: δ_{ip}C(2)H, δ_{ip}C(6)H, δ_{ip}C(5)H, δ_{ip}N(11)H, δ_{ip}N(1)H [5%], δ_{ip}C(8)H.
1613	this stretching mode in quinoline ring is disturbed by a C(4)-N(11) stretching mode. While νC(7)═C(8) [6%], νC(5)═C(10), νC(4)═C(3) and νN(1)═C(2) [5%] stretch in phase along the nuclear bonding axis, νC(2)═C(3) [22%] and C(9)═C(10) [5%] vibrate out of phase. Strong in -plane bending takes place at C(4)C(10)C(9) [14%] and C(10)C(4)C(3) [8%] and in-plane CH bendings are present around the ring: δ_{ip}C(2)H [7%], δ_{ip}C(8)H, δ_{ip}N(1)H, δ_{ip}C(3)H and δ_{ip}N(11)H.
1597	This vibration is mirror image-like in Q1 and Q2 along C(9)-C(10) axis. Modes νC(7)═C(8) [15%] and νC(2)═N(1) [15%] stretch in phase and νC(4)═C(3) [11%] and νC(6)═C(5) [9%] compress at the same time, while C(9) and C(10) are nearly fixed due to the opposite vibration. This vibration is somewhat perturbed by a C(4)═N(11) stretching vibration. Bond lengths of C(6)═C(7) and C(9)═C(10) are constant. Strong in-plane bendings: δ_{ip}C(5)H, δ_{ip}C(3)H [5%], δ_{ip}N(1)H [17%] and δ_{ip}C(8)H.
1575	In-phase symmetric stretching vibrations are present νC(7)═C(6) [11%], νC(9)═C(10) [8%], νC(10)═C(4) [8%] and νN(11)−C(12) while νC(4)═N(11) [6%], νC(5)═C(10 [5%]), νC(7)═C(8) and νC(8)═C(9) vibrate out of phase. Atoms C(3), C(2) and N(1) have no strong displacement. A very strong NH bending is noticed δN(11)H [18%].
1556	Strong in phase stretching vibrations at the quinoline ring take place at ν(11)-C(4) [25%] and νC(9)═C(10) [13%], while νC(4)═C(3) and νC(2)═C(3) [6%] vibrate out of phase. Due to the strong νN(11)-C(4) vibration along the nuclear bonding axis, angles C(10)C(4)C(9) [13%] and C(10)C(4)C(3) [9%] change strong. Strong in plane bendings are present δ_{ip}C(2)H [8%], δ_{ip}N(1)H and δ_{ip}N(11)H [8%]. The Cl(22) atom is fixed and no strong vibration takes place in the side chain.
1489	νC═C in quinoline; δ_{ip}C(5)H, δ_{ip}C(6)H, δ_{ip}C(8)H, δ_{ip}N(1)H, δ_{ip}N(11)H; δ_{ip}C(6)H; δ_sC(21)H$_3$, ρC(21)H$_3$, δ_sC(14)H$_2$, δ_sC(15)H$_2$, δC(12)H
1421	δ_sC(18)H$_3$, ρC(18)H$_3$, δ_sC(17)H$_2$, δ_sC(15)H$_2$, δ_sC(21)H$_3$, ρC(21)H$_3$, δ_sC(20)H$_3$, ρC(20)H$_3$, δN(11)H, νC═C and δ_{ip}CH quinoline
1407	νC═C and δ_{ip}CH quinoline, δN(11)H
1371	νC═C and δ_{ip}CH quinoline, δN(11)H, δN(16)H, δ_sC(13)H$_2$, δ_sC(21)H$_3$
1336	νC═C and δ_{ip}CH quinoline, δC(12)H, δC(13)H, δC(17)H, δN(16)H, ωC(17)H$_2$, δ_sC(20)H$_2$, δN(19)H
1277	δC(12)H, δC(13)H, δC(14)H, δC(19)H, δN(11)H, δN(16)H, δ_{ip}CH quinoline, τC(17)H$_2$,
1252	νC═C and δ_{ip}CH quinoline, τC(13)H$_2$, τC(17)H$_2$, τC(19)H$_2$, δN(16)H
1210	out of phase ring breathing and δ_{ip}CH quinoline, δN(16)H, τC(13)H$_2$, τC(14)H$_2$, τC(15)H$_2$, τC(17)H$_2$, τC(19)H$_2$, ρC(21)H$_3$, ρC(20)H$_3$, ρC(18)H$_3$,
1175	δN(16)H, ρC(18)H$_3$, ρC(19)H$_3$, ρC(20)H$_3$, ρC(14)H$_2$, ρC(19)H$_2$
1161	δ_{ip}CH isoquinoline, δN(16)H, ωC(13)H$_2$, ρC(15)H$_2$, ρC(17)H$_2$
1101	νC−C and δ_{ip}CH quinoline, νC−Cl, ρC(18)H$_3$, ωC(18)H$_3$, ρC(21)H$_3$, ωC(21)H$_3$, ωC(15)H$_2$,
1088	Strong νC(13)−C(14) [8%], νC(14)−C(15) [6%], δN(16)H, ρC(19)H$_2$, ρC(21)H$_3$ in the side chain as well as out of phase ring breathings at Q1 and Q2 are recognized.
1067	νC−C quinoline, δN(16)H, ωC(18)H$_3$, ωC(20)H$_3$, ρC(17)H$_2$, ρC(19)H$_2$, νC(17)−C(18)
908	out of phase νC−C and δ_{ip}CH quinoline, νN(11)−C(12), ρC(21)H$_3$, ρC(14)H$_2$, ρC(15)H$_2$, ωC(13)H$_2$
759	ring breathing (all atoms, except C(7)) and δ_{ip}CH quinoline, δC(12)H, νC(12)−C(21), ρC(21)H$_3$
721	strong --(CH$_2$)$_n$- rockings at C(13) [12%], C(14) [41%] and C(15) [19%]
663	δ_{ip}CC quinoline (shape of C(10)C(3)C(2)C(9) changes between quadrate and parallelogram), νC(12)−C(21), ρC(14)H$_2$, δC(12)H
596	δ_{ip}CC quinoline (shape of Q2 changes between stretched and compressed hexagon), δC(12)H, νC(7)−Cl(22)
275	out-of-plane butterfly quinoline, ωC(21)H$_3$, τC(12)−C(21), in-phase ρC(13)H$_2$, ρC(14)H$_2$, ρC(15)H$_2$, with τC(12)−C(13), τC(13)−C(14), τC(14)−C(15), τC(19)−C(20)

[a] The atomic numbering scheme is used as shown in Figure 1. The most prominent modes enhanced in the resonance Raman spectra are marked in bold; their atomic displacements are shown in Figure 4 and are discussed in more detail. The quantitative contributions of the normal modes in internal coordinates were derived via a PED calculation based on Wilson GF matrix method.[50] Contributions >5% are given in squared brackets for the most important wavenumbers.

cross section itself is intrinsically enhanced via the $(\omega_{exc.})^4$ dependency and the diffraction limited spatial resolution is improved.

The normalized UV/vis absorption spectrum of chloroquine is shown in Figure 2A and the two UV wavelengths are marked by vertical lines. The absorption spectrum shows characteristic maxima between 210 and 380 nm mainly due to the aromatic ring absorption.

The intensity pattern of the Raman bands between 1500 cm^{-1} and 1650 cm^{-1} differs for the two excitation wavelengths 244 and 257 nm (see Figure 2B). The vibrations appearing in this wavenumber region mainly belong to the quinoline ring (vide infra) and are, therefore, sensitive for $\pi-\pi$-interactions to the hematin target. To discuss the differences quantitatively, a deconvolution of the five normal modes in this wavenumber region was performed. Hereby it was derived that, e.g., the relative enhancement of the band at 1635 cm^{-1} compared to the band at 1597 cm^{-1} is more than 4 times stronger for an excitation wavelength of 244 nm compared to 257 nm. Therefore, the excitation wavelength 244 nm should be applied if one is interested to selectively study the mode at 1635 cm^{-1}. A quantitative comparison of the intensity patterns observed for the two deep UV wavelengths is summarized in Table 1. Such a selective enhancement by choosing the appropriate Raman excitation wavelengths makes it possible to monitor vibrational modes of characteristic molecular groups involved

TABLE 3: Comparison of Significant Different Angles and Distances in Chloroquine (CQ) and Chloroquine Protonated at N1 and N16 (CQ2p) as Shown in Figure 1[a]

labeling (atom numbers)	value in CQ	value in CQ2p
	Angles/°	
A1 (9, 1, 2)	116.2	122.4
A2 (3, 2, 1)	125.6	121.5
A3 (10, 4, 3)	116.8	117.9
A4 (4, 10, 9)	117.8	118.9
A5 (10, 9, 1)	123.9	119.0
A6 (7, 8, 9)	120.2	119.2
A7 (10, 9, 8)	119.2	121.7
A8 (5, 10, 9)	118.4	117.0
A9 (12, 11, 4)	125.1	126.8
	Distances/pm	
D1 (1, 2)	131.8	134.0
D2 (2, 3)	140.5	137.5
D3 (3, 4)	139.3	141.4
D4 (10, 9)	142.9	141.9
D5 (1, 9)	136.3	137.8
D6 (9, 8)	141.9	140.3
D7 (7, 8)	137.3	138.3
D8 (22, 7)	174.6	171.7
D9 (4, 11)[b]	136.6	134.4
D10 (11, 12)[b]	145.9	146.9
D11 (15, 16)	146.1	151.2
D12 (16, 19)	146.4	151.9
D13 (16, 17)	146.3	152.0

[a] All shown distances are different by more than 1 pm and all angles are different for equal or more than 1°. [b] Values of distances D9 (4, 11) and D10 (11, 12) in chloroquine protonated at N1, N16, and N11 are D9 = 147.9 pm, D10 = 156.5 pm.

in the drug-target complex formation and, therefore, to study how these modes are influenced because of docking processes in future drug-target-interaction experiments.

The resonance Raman spectra of 1 mM solutions of chloroquine were recorded for pH values of 7.4 and 5 corresponding to the pH values in blood and inside the acid food vacuole, respectively (see Figure 2B). A strong enhancement of the mode at 721 cm^{-1} can be seen for a pH value of 5, while this band is very weak at a pH value of 7.4. Furthermore, a shoulder at 1088 cm^{-1} can be seen in the spectrum of chloroquine at a pH value of 7.4 under excitation with 257 nm, which is missing in the corresponding Raman spectrum at a pH value of 5. These pronounced differences between the Raman spectra recorded for different pH values make it possible to clearly identify whether chloroquine is present under conditions representing pH values inside or outside the acid food vacuole of plasmodium.

To interpret the differences in the Raman spectra recorded for different pH values and under different resonant enhancement conditions, a clear mode assignment is required. While it is possible to approximately assign the vibrations to distinct characteristic normal modes via their typical group wavenumbers, it is impossible to obtain an exact atomic displacement picture without the support of ab initio calculations. This is even more true because the local symmetry in the quinoline is disturbed by the Cl(22) atom and the C(4)N(11) bond (see Figure 1). The assignment of the normal modes and the discussion of the displacements, however, is a very important insight into the molecular behavior. Therefore, the DFT calculation of chloroquine at different protonation states and the vibrational mode assignment will be given in the following chapter.

Density Functional Theory Calculation of Chloroquine at Different Protonation States. As mentioned in the Introduction, the pH trapping effect of the weak base chloroquine (pK_{a1} = 10.2, pK_{a2} = 8.4) in the acid food vacuole of plasmodium was recognized to be of utmost importance for an accumulation and, therefore, for its effectivity.[14−16] Furthermore the protonation state of chloroquine might also be important for its docking properties to the target hemozoin. The structure of the substance chloroquine diphosphate, which was used for the measurement of the experimental non-resonant Raman spectrum is known to be protonated at N1 and N16.[53] Therefore, the situation inside the food vacuole (where chloroquine is expected to be protonated at N1 and N16 because of the pH 5 value) is well resembled. It would be helpful if the influence of the protonation of chloroquine at N1 and N16 can significantly be reflected in the Raman spectrum. Therefore, we present a detailed theoretical examination of the influence of the protonation state of chloroquine on its vibrational spectra, structural parameters like bond length and angles, and molecular orbitals. All calculations have been performed on fully optimized geometries.

Discussion of Vibrational Spectra and Molecular Motions. Figure 3 compares the experimental non-resonant Raman spectra of chloroquine diphosphate (Figure 3G) with the DFT calculated Raman spectra (B3PW91/6-31+G(d,p)) of chloroquine in its unprotonated state (Figure 3F), protonated at N1 (Figure 3E); at N16 (Figure 3D); at N1 and N16 (Figure 3C); and at N1, N16, and N11 (Figure 3B). While the calculation of the unprotonated form (Figure 3F) resembles the Raman bands at 1371 and 759 cm^{-1}, several other significant features like, e.g., the bands at 1101 cm^{-1} and in the interesting wavenumber region between 1500 and 1650 cm^{-1} are not well reproduced by the calculation. Calculations performed with the larger triple split valence basis set 6-311++G(d,p) prove that the observed discrepancies between the calculated and experimentally observed Raman spectra within these important wavenumber regions are not due to finite basis set effects. Therefore, in order to check if these discrepancies originate from the protonation state of chloroquine, calculations of differently protonated chloroquine molecules were performed.

Protonation of chloroquine only at N16 does not permit a better agreement between the calculated and the experimental Raman spectra (Figure 3D). The protonation of chloroquine at N1 (Figure 3E) leads to a significant improvement by reproducing the wavenumber region between 1500 cm^{-1} and 1650 cm^{-1} and also the spectral feature 759 cm^{-1}. However the calculation of chloroquine protonated at N1 and at N16 (Figure 3C) is improved (e.g., the band located at 1101 cm^{-1}) and yields the best overall agreement between the experimental and the calculated Raman spectra. The differences between the calculated Raman spectra of unprotonated chloroquine (Figure 3F) and chloroquine protonated at N1 and at N16 (Figure 3C) are most pronounced in the wavenumber region dominated by molecular vibrations of the quinoline ring system (1500−1650 cm^{-1}). These molecular vibrations are of particular relevance because of their sensitivity to the formation of the $\pi-\pi$-interaction of chloroquine with the porphyrin system of hematin. These modes can be accessed selectively by utilizing different resonance Raman enhancement conditions and, therefore, display promising marker bands for future in vivo docking studies.

To exclude the unlikely situation of chloroquine protonated at N1 and at N16 as well as at N11 (pK_{a3} = 5.0[23]), this structure was also calculated (see Figure 3B). It can be seen that the calculated Raman spectrum of such a triply protonated chloroquine molecule differs significantly from the experimentally observed Raman spectrum. Many main features (e.g., the strong band at 1371 cm^{-1}) are shifted and various new bands, especially in the low wavenumber region, arise. This result can

be understood by considering the molecular geometry of such a triply protonated system where the C4−N11 and N11−C12 bond lengths are significantly increased by approximately 10 pm compared to the unprotonated form, thus separating the molecule into a quinoline ring and a side chain.

To evaluate the role of a water environment, DFT calculations of chloroquine embedded in a water environment treated within the framework of an isodensity polarized continuum model[39] were also performed (see Figure 3A). However taking into account a water environment does not lead to a better agreement between the calculated spectra of the unprotonated form and the experimentally observed spectra. This is another indication that the ionic structure of the doubly protonated chloroquine at N1 and N16 is the right one.

Calculations of the IR absorption spectra yielded the same results; the best agreement between experimental and calculated IR spectra is obtained for the calculation of chloroquine protonated at N1 and at N16. Also the calculations performed with B3LYP lead to the same results as the calculations with B3PW91.

Altogether, the DFT calculations of chloroquine lead to the right result that the experimental spectrum of chloroquine diphosphate is nicely given by the calculation of chloroquine protonated at N1 and N16 in agreement to.[53] The fully optimized molecular geometry and the atomic displacements of the normal modes of doubly protonated chloroquine are used for a detailed discussion of the most important vibrational modes.

The bands in the deep-UV Raman spectra exhibiting the highest intensity are located in the wavenumber region between 1650 and 1500 cm^{-1} (see Figure 2B). The atomic displacements of the five bands in this wavenumber region are shown in Figure 4A. One can clearly recognize the localization of the modes within the quinoline ring system. All modes are dominated by C═C stretching modes and CH in-plane bending modes. No significant atomic displacement within the chloroquine side chain contributes to these vibrations. These modes are, therefore, promising candidates for investigating the $\pi-\pi$ interactions of chloroquine with hemozoin by analyzing possible changes in this wavenumber region due to a docking process.

The resonance Raman spectra of chloroquine measured at a pH value of blood (pH 7.4) and at the pH value inside the acid food vacuole (pH 5) are distinguishable on the basis of the shoulder at 1088 cm^{-1} (in case of $\lambda_{exc.} = 257$ nm) and the bands at 721 cm^{-1} (see Figure 2B). The atomic displacements of the modes at 720 cm^{-1} and 1088 cm^{-1} are shown in Figure 4B. These modes are characterized by strong in-phase -$(CH_2)_n$- rocking vibrations in the side chain near N16. This localization near N16 verifies very well the suggested changes in this part of the molecule because of the protonation of N16. A change of protonation of N16 takes place when the pH value of the environment changes, e.g., from pH 7.4 (blood) to pH 5 (acid food vacuole).

The role of the Cl(22) atom (bonded to the C(7) atom of the quinoline ring) for the docking properties of chloroquine is discussed in the literature.[12] The presented calculations show that the Cl atom is almost fixed in space, showing only slight displacements for a few normal modes, while the Cl atom influences the quinoline vibrations in terms of disturbing their symmetry.

Potential energy distribution (PED) calculations based on the Wilson GF matrix method were also performed to obtain a quantitative decomposition of the normal modes in intuitive internal coordinates. A complete vibrational assignment of all prominent vibrational bands is summarized in Table 2.

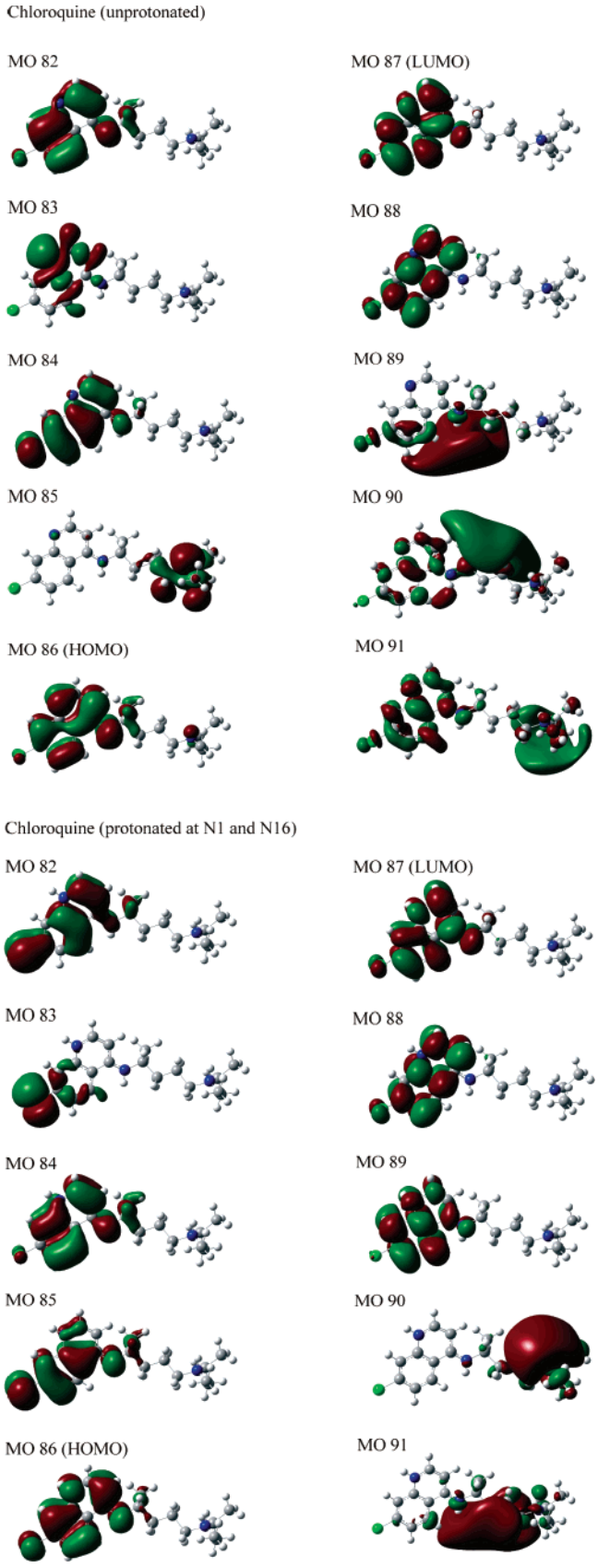

Figure 5. Comparison of the five highest occupied (MO 82 − 86) and the five lowest unoccupied (MO 87−91) molecular orbitals of chloroquine unprotonated and protonated at N1 and N16 (see Figure 1).

Discussion of Bond Lengths and Angles. The observed differences in the calculated Raman spectra of chloroquine for different protonation states are manifested in other structural

parameters like bond length and angles, too. Various bond lengths and angles within the quinoline ring change significantly upon protonation. All bond lengths that change more than 1 pm and angles that change more than 1° upon protonation are summarized in Table 3. As one might have expected the N1 atom in unprotonated chloroquine is placed outside the ideal hexagon and the corresponding angle A1 (116°) is much smaller than the ideal 120° value. Due to protonation the N1 atom moves significantly inside the hexagon, and accordingly the angle A1 changes to 122° influencing all surrounding bond lengths and angles significantly. Thus protonation approaches the hexagon more toward an ideal shape. The bond distances at the beginning of the side chain are also changed and all three bond lengths around N16 are significantly elongated upon protonation.

Discussion of Molecular Orbitals. The differences in the spectral patterns of the resonance Raman spectra of chloroquine excited with the two UV excitation wavelengths at 244 and 257 nm and the differences for chloroquine measured at pH 5 compared to pH 7.4 (Figure 2B) are further understood by considering the significant changes in relevant parts of the molecular orbitals of the unprotonated and doubly protonated forms of chloroquine. The five highest occupied molecular orbitals (MO 82−86) and the five lowest unoccupied orbitals (MO 87−91) of unprotonated chloroquine and chloroquine protonated at N1 and N16 are compared in Figure 5, whereas MO 86 is considered as the HOMO and MO 87 as the LUMO. As expected, the HOMO−LUMO transition is mainly located in the quinoline ring system. However transitions to higher MOs involving also the side chain, indicate to include these parts of the molecule into the discussion of vibrations enhanced under resonance conditions. Differences in molecular parts of the side chain for unprotonated chloroquine and chloroquine protonated at N1 and at N16 are best seen at MOs 85, 89, 90, and 91. The resonance enhancement in the Raman spectra can, therefore, qualitatively be understood by analyzing the molecular orbitals.

Conclusion

This paper shows that the UV resonance Raman spectra of chloroquine recorded for pH values resembling conditions in the blood and in the acid food vacuole of plasmodium can be distinguished. The (parameter-free) DFT calculations of chloroquine for different protonation states elucidates that the experimental vibrational spectra are best resembled by the calculated spectrum of the doubly protonated form, in agreement with ref 53. The changes within the calculated Raman spectra for the different protonation states are significant and are manifested by dramatic changes of bond lengths and angles upon protonation. These differences are certainly crucial for molecular interactions to the biological target molecules. The calculation of the atomic displacements for the most significant normal modes within the experimental spectra yields valuable insights into the molecular vibrations.

The presented results suggest that UV resonance Raman micro spectroscopy is an extremely capable method to localize chloroquine inside the acid food vacuole of plasmodium. Resistant strains of plasmodium are characterized by a slight increase of the pH value inside the acid food vacuole. The Raman results presented within this study open up the interesting possibility to study such pH changes in vivo by means of deep UV Raman spectroscopy. In addition, the information derived within this study is essential for the interpretation of upcoming in-vitro and in-vivo studies of the interaction process of chloroquine with its biological target molecules, hematin and hemozoin. It will be interesting to observe the changes of the selective enhanced molecular vibrations within chloroquine due to the docking process. Direct monitoring of this docking process will help to understand the mode of action of chloroquine at a molecular level and produce the necessary knowledge for a specific design of new tailor-made antimalarials and the fight against growing resistances against anti-malaria active agents.

Acknowledgment. We gratefully acknowledge support from the Fonds der Chemischen Industrie and the Deutsche Forschungsgemeinschaft (Sonderforschungsbereich 630 “Recognition, Preparation, and Functional Analysis of Agents Against Infectious Diseases”, projects C1 and A2).

Supporting Information Available: Further details shown in four figures. This material is available free of charge via the Internet at http://pubs.acs.org.

References and Notes

(1) Hastings, I. M.; Bray, P. G.; Ward, S. A. *Science* **2002**, *298*, 74−74.

(2) Wellems, T. E. *Science* **2002**, *298*, 124−126.

(3) Ridley, R. G. *Nature* **2002**, *415*, 686−693.

(4) Foley, M.; Tilley, L. *Pharmacol. Ther.* **1998**, *79* (1), 55−87.

(5) Francis, S. E.; Sullivan, D. J., Jr.; Goldberg, D. E. *Annu. Rev. Microbiol.* **1997**, *51*, 97−123.

(6) Ursos, L. M. B.; Roepe, P. D. *Med. Res. Rev.* **2002**, *22* (5), 465−491.

(7) Wiesner, J.; Ortmann, R.; Jomaa, H.; Schlitzer, M. *Angew. Chem.* **2003**, *115*, 5432−5451.

(8) Sullivan, D. J., Jr.; Matile, H.; Ridley, R. G.; Goldberg, D. E. *J. Biol. Chem.* **1998**, *273* (47), 31103−31107.

(9) Sullivan, D. J., Jr.; Gluzman, I. Y.; Russell, D. G.; Goldberg, D. E. *Proc. Nat. Acacd. Sci. USA* **1996**, *93*, 11865−11870.

(10) Ridley, R. G.; Hofheinz, W.; Matile, H.; Jaquet, C.; Dorn, A.; Masciadri, R.; Jolidon, S.; Richter, A.; Guenzi, M.; Girtometta, W. F.; Urwyler, H.; Huber, W.; Thaithong, S.; Peters, W. *Antimicrob. Agents Chemother.* **1996**, *40*, (8).

(11) Cheruku, S. R.; Maiti, S.; Dorn, A.; Scorneaux, B.; Bhattacharjee, A. K.; Ellis, W. Y.; Vennerstrom, J. L. *J. Med. Chem.* **2003**, *46*, 3166−3169.

(12) Egan, T. J.; Hunter, R.; Kaschula, C. H; Marques, H. M.; Misplon, A.; Walden, J. *J. Med. Chem.* **2000**, *43*, 283−291.

(13) Kaschula, C. H.; Egan, T. J.; Hunter, R; Basilico, N.; Parapini, S; Taramelli, D.; Pasini, E.; Monti, D. *J. Med. Chem.* **2002**, *45*, 3531−3539.

(14) Olivaro, P. L.; Goldberg, D. E.; *Parasitol. Today* **1995**, *11*, (8), 294−297. Hawley, S. R.; Bray, P. G.; O’Neill, P. M.; Park, B. K.; Ward, S. A. *Biochem. Pharmacol.* **1996**, *52*, 723−733.

(15) Yayon, A.; Cabantchik, Z. I.; Ginsburg, H. *EMBO J.* **1984**, *3*, (11), 2695−2700.

(16) Ginsburg, H.; Geary, T. G. *Biochem. Pharmacol.* **1987**, *36*, (10), 1567−1576.

(17) Leed, A.; DuBay, K.; Ursos, L. M. B.; Sears, D.; de Dios, A. C.; Roepe, P. D. *Biochemistry* **2002**, *41*, 10245−10255.

(18) de Dios, A. C.; Tycko, R.; Ursos, L. M. B.; Roepe, P. D. *J. Phys. Chem.* A **2003**, *107*, 5821−5825.

(19) Constantinidis, I.; Satterlee, J. D. *J. Am. Chem. Soc.* **1988**, *110*, 927−932.

(20) Constantinidis, I.; Satterlee, J. D. *J. Am. Chem. Soc.* **1988**, *110*, 4391−4395.

(21) Frosch, T.; Küstner, B.; Schlücker, S.; Szeghalmi, A.; Schmitt, M.; Kiefer, W.; Popp, J. *J. Raman Spectrosc.* **2004**, *35*, 819−821.

(22) Pagola, S.; Stephens, P. W.; Bohle, D. S.; Kosar, A. D.; Madsen, S. K. *Nature* **2000**, *404*, 307−310.

(23) Buller, R.; Peterson, M. L.; Almarsson, Ö.; Leisirowitz, L. *Crystal Growth Des.* **2002**, *2*, (6), 553−562.

(24) Frisch, M. J.; Trucks, G. W.; Schlegel, H. B.; Scuseria, G. E.; Robb, M. A.; Cheeseman, J. R.; Zakrzewski, V. G.; Montgomery, J. A., Jr.; Stratmann, R. E.; Burant, J. C.; Dapprich, S.; Millam, J. M.; Daniels, A. D.; Kudin, K. N.; Strain, M. C.; Farkas, O.; Tomasi, J.; Barone, V.; Cossi, M.; Cammi, R.; Mennucci, B.; Pomelli, C.; Adamo, C.; Clifford, S.; Ochterski, J.; Petersson, G. A.; Ayala, P. Y.; Cui, Q.; Morokuma, K.; Malick, D. K.; Rabuck, A. D.; Raghavachari, K.; Foresman, J. B.; Cioslowski, J.; Ortiz, J. V.; Stefanov, B. B.; Liu, G.; Liashenko, A.; Piskorz, P.; Komaromi, I.; Gomperts, R.; Martin, R. L.; Fox, D. J.; Keith, T.; Al-Laham, M. A.; Peng, C. Y.; Nanayakkara, A.; Gonzalez, C.; Challacombe, M.; Gill, P. M.

W.; Johnson, B. G.; Chen, W.; Wong, M. W.; Andres, J. L.; Head-Gordon, M.; Replogle, E. S.; Pople, J. A. *Gaussian 98*, revision A.11.4; Gaussian, Inc.: Pittsburgh, PA, 1998.

(25) Becke, A. D. *J. Chem. Phys*. **1992**, *97*, 9173; Becke, A. D. *J. Chem. Phys.* **1993**, *98*, 5648.

(26) Stephens, P. J.; Devlin, F. J.; Chabalowski, C. F.; Frisch, M. J. *J. Phys. Chem.* **1994**, *98*, 11623.

(27) Lee, C.; Yang, W.; Parr, R. G. *Phys. Rev.* **1988**, *B37*, 785.

(28) Perdew, J. P.; Wang, Y. *Phys. Rev.* **1992**, *B45*, 13244; Perdew, J. P.; Chevary, J. A.; Vosko, S. H.; Jackson, K. A.; Pederson, M. R.; Singh, D. J.; Fiolhais, C. *Phys. Rev.* **1992**, *B46*, 6671.

(29) Neugebauer, J.; Hess, B. A. *J. Chem. Phys*. **2003**, *118*, (16), 7215−7225.

(30) Scott, A. P.; Radom, L. *J. Phys. Chem.* **1996**, *100*, 16502−16513.

(31) El-Azhary, A. A.; Suter, H. U. *J. Phys. Chem*. **1996**, *100*, 15056−15063.

(32) Baker, J.; Jarzecki, A. A.; Pulay, P. *J. Phys. Chem A* **1998**, *102*, 1412−1424.

(33) Rauhut, G.; Pulay, P. *J. Phys. Chem.* **1995**, *99*, 3093−3100.

(34) Halls, M. D.; Schlegel, B. *J. Chem. Phys*. **1998,** *109*, (24), 10587−10593.

(35) Andersson, M. P.; Uvdal, P. *J. Phys. Chem. A* **2005**, *109*, 2937−2941.

(36) Pople, J. A.; Schlegel, H. B.; Krishnan, R.; Defrees, D. J.; Binkley, J. S; Frisch, M. J.; Whitside, M. J. *Int. J. Quantum Chem., Quant. Chem. Symp*. **1981**, *15*, 269−278; Frisch, M. J.; Pople, J. A.; Binkley, J. S. *J. Chem. Phys*. **1984**, *80*, (7), 3265−3269 and references therein; Hehre, W. J.; Stewart, R. F.; Pople, J. A. *J. Chem. Phys*. **1969**, *51*, (6), 2657−2664 and references therein.

(37) Boese, A. D.; Martin, J. M. L. *J. Chem. Phys*. **2003**, 119, (6), 3005−3014.

(38) Wiberg, K. B. *J. Comput Chem* **2004**, *25*, 1342−1346.

(39) Tomasi, J.; Mennucci, B.; Cammi, R. *Chem. Rev.* **2005**, *105*, 2999−3093.

(40) Figgen, D.; Metz, B.; Stoll, H.; Rauhut, G. *J. Phys. Chem. A* **2002**, *106*, 6810−6816.

(41) Liu, R.; Zhou, X.; Pulay, P. *J. Phys. Chem.* **1992**, *96*, 8336−8339.

(42) Fogarasi, G.; Zhou, X.; Taylor, P. W.; Pulay, P. *J. Am. Chem. Soc.* **1992**, *114*, 8191−8201.

(43) Forgarasi, G.; Pulay, P. *J. Mol. Struct.* **1986**, *141*, 145−152.

(44) Pulay, P.; Fogarasi, G.; Pang, F.; Boggs, J. F.; Vargha, *A. J. Am. Chem. Soc*. 1983, *105*, 7037−7047.

(45) Pulay, P.; Fogarasi, G.; Pang, F.; Boggs, J. F. *J. Am. Chem. Soc*. **1979**, *101*:*10*, 2550−2560.

(46) Wong, M. W. *Chem. Phys. Lett.* **1996**, *256*, 391−399.

(47) Bauschlicher, C. W.; Langhoff, S. R. *Spectrochim. Acta, Part A* **1997**, *53*, 1225−1240.

(48) Halls, M. D.; Velovski, J.; Schlegel, H. B. *Theor. Chem. Acc.* **2001**,*105*, 43−421.

(49) Long, D. A. The Raman Effect; Wiley: New York, 2002.

(50) Bright, W. E., JR. *J. Chem. Phys*. **1941**, *9*, 76−84.; Bright W. E., JR. *J. Chem. Phys*. **1939**, *7*, 1047−1052.; Wilson, E. B.; Decius, J. C.; Cross, P. C. *Molecular Vibrations*; McGraw-Hill: New York, 1955.

(51) Martin, J. M. L.; Van Alsenoy, C. GAR2PED.

(52) McHale, J. L. In *Handbook of Vibrational Spectroscopy*; Wiley: New York, 2002; Vol 1, and references therein.

(53) Karle, J. M.; Karle, I. L. *Acta Cryst.* **1988**, *C44*, 1605−608.